NOTICE CONCERNING COPYRIGHT RESTRICTIONS

Inexpensive, Automated Micro-Earthquake Data Collection and Processing System for Rapid, High-Resolution Reservoir Analysis

Lawrence Hutchings[1], Steve Jarpe[2], Katie Boyle[1], Gisela Viegas[1], and Ernest Majer[1]

[1]Lawrence Berkeley National Laboratory, Berkeley CA
[2]Jarpe Solutions, Prescott Valley AZ

Keywords

Reservoir analysis, micro-seismicity, automated processing

ABSTRACT

We present an inexpensive, automated micro-earthquake data collection and processing system that provides the ability to quickly and simply perform high-resolution micro-earthquake source parameter and tomographic inversion studies. Such information provides the basis for reservoir analysis. The easily deployable nature of our system allows for potential large-scale assessment of resources in regions throughout the world. Further, the system's low hardware cost, simple operation, and automation make it attractive to small companies and developing countries with little money and few trained personnel to process and analyze data. The system includes: (1) an inexpensive micro-earthquake recorder that requires very little time and no technician input to install, (2) an automated data processing program to manage data, one that requires merely placing flash memory chips (or telemetry) into a computer, (3) automated creation of meta-data that provides preliminary earthquake locations, moments, magnitudes, and input files for tomography and earthquake source studies, and (4) an interactive program for testing micro-earthquake network designs for accuracy and resolution. Final analysis requires a trained professional to obtain reliable results, including final source parameters, 3D-velocity structure (V_p and V_s)**,** and 3D-attenuation structure **(**Q_p and Q_s). These results are arranged into input files that enable VisIt visualization software to carry out GUI analysis. This data analysis is intended for use in reservoir monitoring and near-real-time modeling of reservoir properties. A companion paper, Bonner et al., (2011), describes how this information is used, along with the rock physics necessary to interpret reservoir properties.

Introduction

Recordings of micro-earthquakes can provide a valuable tool for evaluating geothermal reservoirs, which often occur at depths or in heterogeneous geological environments that preclude using other methods. Further, the accurate locations of micro-earthquakes have proven to be extremely useful in monitoring hydro-fracking during the creation of reservoirs. Imaging reservoirs requires sufficient numbers of micro-earthquakes to resolve the geologic structure and its properties. Sparsity of micro-earthquakes can result in inadequate data coverage or a too-long data gathering period to make the recordings useful. Further, the expense of setting up recorders for accurate micro-earthquake locations during hydro-fracking can be prohibitive. Hutchings (2011) showed that the sparsity of micro-earthquakes can be compensated for by increasing the number of recording stations for tomography studies, which also improves earthquake location accuracy. Increasing stations would therefore significantly improve reservoir evaluation, exploitation, and resource management capabilities, if it could be done at a reasonable cost in time and dollars. Here, we present an inexpensive, automated micro-earthquake data collection and processing system that can cost effectively use many stations and thus provide the ability to quickly and simply perform high-resolution micro-earthquake source parameter and tomographic inversion studies. This information provides the basis for reservoir analysis.

The system includes: (1) an inexpensive micro-earthquake data acquisition system that requires very little time and no technician input to install, (2) an automated data processing and managament program that requires merely putting flash memory chips (or telemetry) into a computer, (3) automated meta-data processing that provides preliminary earthquake locations, moments, magnitudes, and input files for tomography and earthquake source studies, and (4) an interactive program for testing micro-earthquake network designs for accuracy and resolution. This entire package is called the Rapid Reservoir Assessment System (RRAS).

Obtaining reliable meta data cannot be automated, and requires a trained professional, these include: final source parameters, 3D-velocity structure (V_p and V_s)**,** and 3D-attenuation structure **(**Q_p and Q_s). These results are arranged into input files that enable VisIt visualization software to conduct GUI analysis. This data analysis is intended for use in reservoir monitoring and near-real time modeling of reservoir properties. Here we show an example

of how this data is used to obtain reservoir properties. A companion paper Bonner et al., (2011) describes how this information is used, along with the requisite rock physics to interpret reservoir properties.

The inexpensive, easily deployable, and automated data management of our system additionally allows (1) for potential large scale assessment of resources in regions throughout the world and (2) small companies and developing countries with little money and few trained personnel to achieve sophisticated reservoir analysis. The LBNL RRAS has been developed by the U.S. Department of Energy over several years and is available for technology transfer. The approach of using inexpensive field instrumentation with automated data processing and extracting seismological information from micro-earthquakes was first implemented by Majer and McEvilly (1982). We have expanded on this approach.

The RRAS is primarily directed towards surface or shallow borehole recordings. While surface recordings have the drawback that the signal-to-noise ratios (SNR) can be considerably lower than borehole recordings, and smaller events may not be sufficiently recorded. Of course, we cannot identify the conditions under which one can expect to have micro-earthquakes to analyze or the number that will likely occur, still the RRAS can potentially provide information heretofore unattainable or affordable to many organizations and countries around the world.

Data Acquisition System

The data acquisition system (Figure 1) consists of a data recorder, three orthogonally mounted 4.5 or 8.0 Hz geophones suitable for installation at the surface or in shallow boreholes, GPS receiver, and a solar panel for charging the batteries. The components are coordinated with an inexpensive but powerful microcontroller with very low power consumption.

The data recorder includes a 24-bit delta-sigma ADC digitizer with 18-bit effective resolution on each sensor component. GPS signals provide timing synchronization and self-location of the recording station. A small rechargeable 12-volt gel cell battery (10×10×7 cm, 2 kg) with 5-watt solar panel can power the system indefinitely. The total cost of the acquisition system is $1500.

Event-detected or continuous sensor data is recorded on easily removable standard SD flash memory cards (used in cameras and other electronics), or by radio telemetry (at extra cost). At 500 sps continuous recording requires 0.5 Gb per day on a flash memory card, and at 300 sps, it is 0.3 Gb per day—much more than when in event detection mode. Processing memory cards will take about 15 minutes per Gb, but several can be run simultaneously.

The user interface consists of a small LCD screen, a knob, and several buttons. The screen displays status information—such as whether the system is powered up and running, whether the GPS is locked onto enough satellites to provide a location estimate and/or timing, and how much memory has been used. The knobs and buttons are used to set station parameters such as sample rate and recording mode. The simple on-system user interface was chosen over an interface based on an external computer in order to reduce cost and complexity, and to increase reliability.

The system setup can be done in the laboratory prior to deployment, or in the field if necessary. Installation requires merely setting the sensor in good contact with the ground, placing the recording unit on the ground or mounting it on a stake, and then turning the system on. Periodic station maintenance (i.e., every 2 weeks) consists of replacing the current SD card with an empty card. A simple utility is provided so that the operator can insert a data memory card into a PC and view seismograms and statistics (number of events, etc.).

Figure 1. Data logger, top left; borehole sensor, bottom left; protective case with data logger, battery, and GPS, and solar panel, right.

Automated Data Processing and Management System

The micro-earthquake data processing and management system is an easy-to-use automated system that operates on a common personal computer or laptop. The system is equipped to accept either telemetered or nontelemetered data from recording stations. The following processing steps are used:

1. identify recordings of earthquakes and extract a short segment of seismic data from the raw data files. If the recordings are event-detected, the raw data will already be divided into files containing the segments.
2. Extract some characteristics from each segment, such as station location, time of beginning, peak, end of significant energy above the noise level, and store them in a database table. Instrument response parameters associated with each segment are also stored in the database.
3. Associate segments from different stations into events. An event is a common ground motion source resulting in energy arriving at multiple recording stations. Criterion for an event is window begin times within a maximum time interval at a minimum number of recording stations.
4. Store some characteristics of the event, such as recording station, total energy of event (sum of window energy in associated segments, time of the earliest segment window [w-time]). An event identification is assigned to the event.

Arrival-Time-Picking

Critical to high resolution is accuracy of arrival time picks for both P- and S-waves—crucial for obtaining accurate earthquake locations, 3D velocity and Q models, and attenuation estimation. We invested a considerable amount of time developing an automated picker to improve the accuracy of identifying the time of first arrivals. Once these are identified, then the system also obtains amplitudes, pulse widths, direction of motion, and spectral segments of the P- and S-waves.

The basis of the picker ("Katie pick") is a series of subroutines meant to replicate the deterministic capabilities of the human picker. Several previously developed pickers are implemented in a series of steps leading up to the final pick. P- and S-waves are picked based on the short-term and long-term averages of a characteristic function for each seismic record (Allen, 1978), McEvilly and Majer's approach (1982), subroutine Piki.f (Crosson, 1975), along with internal "artificial intelligence" logic. The picking algorithm then assigns emergence characteristics, confidence values, and direction of first motion. All programs are written to allow the user to define important threshold values for the auto-picker. In this way, though the picker is automated, it still allows the user a high degree of control over the way in which data are analyzed. To test the picking algorithm, we hand picked 1000 seismograms to test the effectiveness of the auto-picker. We found the auto-picker to be consistent with the hand picks 95% and 75% of the time for P-waves and S-waves to the same digital sampling value, respectively. However, when they differed, we often preferred the auto-pick.

The auto-picker is programmed to first locate the P-arrival and to use that value to create a suitable window in the horizontal records for the S-arrival. Vertical records were used to pick P-arrivals. The P pick is limited to a window around the segment energy window to prevent early picks. (We don't use seismograms where no P-pick was identified.) S-waves are picked separately on each component, using the P pick from the vertical component to constrain the search window; if they are significantly different and of good quality, they are preserved for shear wave splitting studies (in progress). Picks are screened by computing a preliminary location using a simple algorithm and eliminating picks that are not consistent with a single best-fit location. Figure 2 shows an example of an S-wave picked automatically.

For the purposes of our high-precision locations and tomography calculations, only the highest quality events are selected. The rationale is that we do not try to locate every earthquake, but rather a good set of high-quality events. For this reason, we choose strict criteria for an event to be used and count on the high density of the network to obtain enough good arrivals over a relatively short time. However, the system does process, locate, and store each event that has enough picked arrivals to compute a location (insert an estimate of SimulPS's minimum requirements for computing a location).

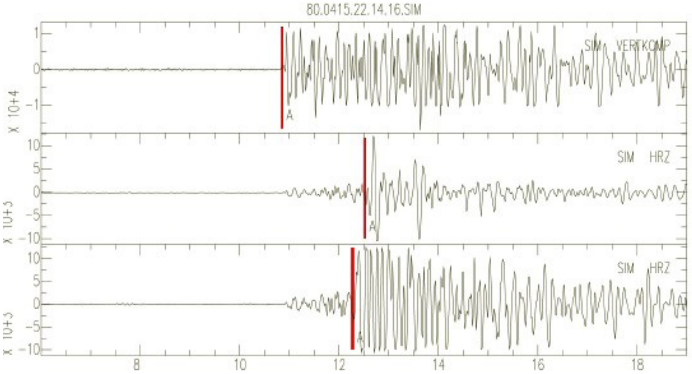

Figure 2. Typical P- and S-wave picks. Notice the time difference between S-picks on two components.

Meta-Data Processing

We use several computer codes to develop meta-data and prepare input files for inversion codes. First, we run SimulPS (discussed below) with a "starting" 3D velocity model to generate a first estimate of the earthquake location. After the initial location has been determined, it is possible to refine auto-picks using the similarity of waveforms with cross-correlation. If the two events are located close to each other and are approximately the same size, then their waveforms should be nearly identical. The formation of cross-correlation pairs is facilitated through the ph2dt program (Waldhauser, 2001). We used a minimum cross-correlation value of 0.85 to improve picks. Figure 3 shows two traces with a cross-correlation value of 0.85. We then use the NetMoment program (discussed below) along with earthquake locations and recorded spectra to get spectral estimates of t*. Finally, we use the moment tensor inversion code TDMT_INVC (discussed below) coupled with the 3D Green's function generation code E3D (discussed below) to obtain moment tensor solutions.

The meta-data is used to compute final locations and create a catalog, and 3D-velocity structure (V_p and V_s) using tomoDD (discussed below). We use program SimulQ (discussed below) to create a 3D attenuation model (Q_p and Q_s). We also use NetMoment along with earthquake locations and recorded spectra to get moment and stress drop. Finally, we use the moment tensor inversion code of Stump and Johnson (1977) to obtain moment tensor solutions. We are in the process of writing a code to invert for anisotropy.

Software for Analysis

HypoDD eliminates much of the uncertainty in relative earthquake locations resulting from poor velocity models (Waldhauser and Ellsworth, 2000). Relative location accuracy generally improves by a factor of 10, from near 1–2 km to 0.1 – 0.2 km.

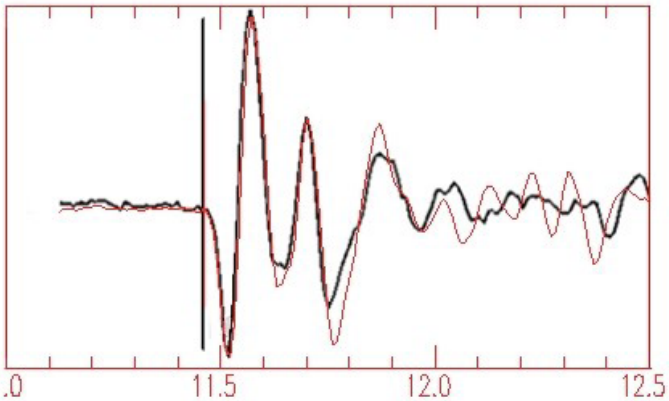

Figure 3. Two traces with a cross-correlation value of 0.85.

Implementation of this code improves delineation of faults or fractures.

SimulPS standard linearized inversion of the nonlinear relations has been performed for years to interpret the geologic structure of local geology. SimulPS (Thurber, 1983) minimizes the misfit between the model slowness and observed first-arrival times, and simultaneously solves for earthquake location and three-dimensional velocity structure. SimulPS accounts for station elevation (and/or station corrections) and borehole depths.

TomoDD combines the two codes Simul and HypoDD to obtain greater relative location accuracy between events and more accurate tomographic inversion results (Zhang and Thurber, 2007).

NetMoment conducts a simultaneous inversion for moment, source corner frequency, and site-specific spectral attenuation t^* (Hutchings, 2002). The simultaneous inversion is based upon the assumption that corrected long period spectral levels and the source corner frequencies from a particular earthquake will have the same value at each site, so that differences in spectra are caused by propagation path and individual site-attenuation effects, t^*

SimulQ, modified from simulPS, performs a liner tomographic inversion of t^* for three-dimensional Q_p *and* Q_s structure (Zucca et al., 1994). The final velocity model and earthquake locations are used and held fixed to allow for the liner inversion. We obtain time domain t^* from pulse widths of initial P- and S-waves from our auto-picker and obtain spectral estimates from program NetMomnet.

Moment Tensor Inversion is obtained from a full-waveform linear inversion for source time function and all moment tensor components, following Stump and Johnson (1977).

TDMT_INVC (Time-Domain Moment Tensor INVerse Code) performs a time-domain full-waveform inversion to obtain the complete static moment tensor solution. The code developed by Dreger (*Minson and Dreger*, 2008) solves for both the directivity and isotropic source components. Non-double-couple moment tensor solutions have been observed in volcanic- and geothermal-induced earthquakes, and its identification can help decipher the physical mechanism of the rupture.

E3D is a 3D elastic finite-difference seismic wave propagation code developed by Larsen and Schultz (1995). E3D capabilities are used to generate source-stations 3D Green's function for the moment tensor inversion. The crustal model is defined from the final 3D-velocity structure and 3D attenuation model obtained with the tomographic inversions.

EFMS automatically estimates the focal mechanism solutions from first motion data.

Network Accuracy and Resolution Evaluation Tool

Accuracy and resolution (A & R) are complementary properties necessary to interpret the results of earthquake location and tomography studies. Accuracy is how close an answer is to the "real world". Earthquake location accuracy is how close an earthquake can be located to an actual location. Resolution is often expressed as 95% confidence ellipses, where resolution is how small a confidence ellipse one can achieve. In tomography, we similarly identify accuracy as how close tomographic images are to actual geology, and how small a confidence ellipse can be achieved. A&R are affected by the limitations of the process; including noise in the data, accuracy of the ray tracers, frequency band limits of the recorded data, the geometry of the recording stations, and the tomography or earthquake location method used.

We have developed computational a tools for evaluating A & R for micro-earthquake networks to aid in their design. First, we hypothesize node spacing, number of stations and earthquakes. A node represents a voxel around the node. We also can choose likely numbers of actual recording as a function of magnitude. We calculate the degrees of freedom that can be achieved by any given node spacing, number of stations and earthquakes. We further can calculate synthetic arrival times from synthetic three-dimensional velocity models and earthquake locations. These are the "real" travel times, velocity models, and earthquake locations. We then can perturb travel times with noise, modify the "actual" velocity model, or randomly move hypocenters to replicate a starting location away from the "true" location. We establish travel times with the pseudo-bending ray tracer and use the same ray tracer in the inversion codes. These tools allow users to virtually run their experiment ahead of installation to see what accuracy and resolution are possible.

As an example, assume a 6×6×4 km volume where the micro-earthquakes are distributed randomly between 2.0 and 3.5 km deep. We consider earthquakes from magnitudes of about -1.0 to 3.0. We are assuming we will solve for both P- and S- wave model parameters, and that 75% of the P-arrivals are usable and 50% of the S-arrivals are usable, due to SNR and interference. With this information, we calculate accuracy and resolution. Table 1 shows several measurements of accuracy and resolution for both the Simul and TomoDD inversion codes when one hundred earthquakes are recorded.

Table 1.

id	stations; interval meters	3D node interval; meters	Average erq error simulPS	Average erq error tomoDD	Average vel error simulPS	Average vel error tomoDD	Average Resol. Simul	Average Resol. Tomo
1	9; 1000	1000	0.56	0.45	0.15	0.12	0.12	0.08
2	16; 1000	500	0.27	0.22	0.12	0.16	0.14	0.06
3	25; 800	100	0.15	0.12	0.11	0.15	0.13	0.05
4	36; 666	100	0.14	0.11	0.09	0.14	0.12	0.05
5	72; 333	10	0.1	0.05	0.05	0.14	0.1	0.03

where, following columns across, "stations" is the number of stations and interval is their spacing in meters; 3D "grid interval" is grid node spacing in meters; "Average erq error simulPS (and TomoDD" is the difference between the actual (synthetic) earthquake location and that of the final solution; "Average vel error simulPS (and TomoDD)" is the average difference between the actual (synthetic) and the velocity model value solved for (only well-resolved nodes are used); and Average Resol. Simiul (and TomoDD) is the average standard error calculated for well-resolved velocity nodes. We consider a node with 10 hits or more to be "well resolved." "Degrees of freedom" are described below, and "Average Hits" is the average number of hits per node. These last two values are essentially the same for both codes.

In general, one wants four times the number of observations as parameters. Degrees of freedom are the difference between these numbers. In simultaneous inversion for velocity structure and earthquake location, the number of parameters solved for is

four times the number of earthquakes, plus the number of velocity nodes solved for and possibly station corrections. The number of observations is the number of P- or S-waves observed. We recognize that generally there are more P- than S-waves utilized, so there is a better *qfac* for P-waves than S-waves. Figure 4 shows a three-dimensional plot of the number of stations, number of earthquakes, and node spacing versus the ratio of number of observations to parameters for a 6×6×4 km volume. Examining Figure 4, we see that the combination of number of stations, earthquakes, and node spacing that achieves the desired results are the colors yellow and hotter. So, for example, one can hypothetically achieve 1 km resolution with nineteen stations and 79 events, and 0.5 km resolution with 94 stations and 92 events. Ten-meter resolution can be achieved with 250 stations and 180 earthquakes.

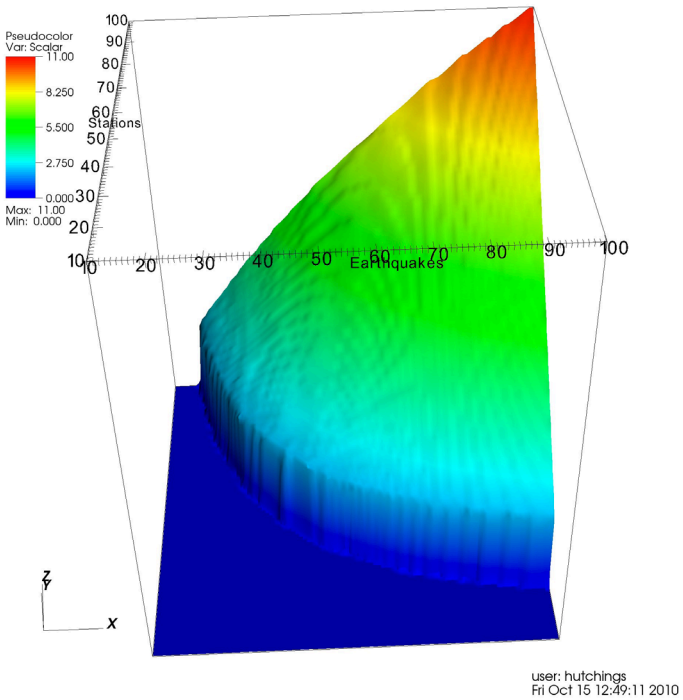

Figure 4. Three-dimensional plot of the number of stations, number of earthquakes, and node spacing versus the ratio of the number of observations to parameters.

Analysis of Meta Data

Rock physics (Gaussman, 1956) along with effective medium theories (Berryman, 1995 & 2007) addresses the relationship among measurements of elastic parameters (which appear in Hooke's law) in the interpretation of fractured and porous media. Interpretation includes mineralogy, porosity, pore shapes, pore fluids, pore pressures, permeability, viscosity, stresses, and overall architecture, such as laminations and fractures (Sayers, 2009). For reservoir-scale interpretations, we primarily use field observables V_p and V_s, and Q_p and Q_s, obtained from tomography studies, in conjunction with borehole logs and laboratory analysis made from surface, well, and lab equipment.

In oil and gas studies, the tool most commonly used to remotely analyze fluid content and fractures is interpretation of seismic wave velocities and attenuation measurements obtained from active seismic sources (Berryman, 2007). We attempt to further these approaches with passive seismic sources. Julian, Evan and Folger have several papers in which they interpret micro-seismic studies using rock physics (1996, 1997, 1999, 2003, 2007). We have previously examined rock physics and effective medium theories to interpret observable data and tomographic images (Zucca et. al., 1993; Berge et al., 2001; and Bonner et al., 2011).

Basic Observations and Assumptions of Rock Physics and Effective Medium Theories

We have reviewed the literature for basic relations in rock physics that pertain to evaluating reservoir properties from analysis of micro-earthquake data. The summary of these results include:

- Increase in velocity and decrease in attenuation with depth due to closing of small cracks caused by increasing pressure from the lithostatic load.
- Decrease in velocity and increase in attenuation due to faulting and fracturing
- Decrease in velocity due to chemical alteration
- Extreme temperature gradient works to decrease velocity with depth
- Fluid saturation acts to stiffen the pores to deformation; affects P-wave velocity, but not S-wave velocity
- Attenuation during seismic wave propagation is due to both extrinsic scattering and intrinsic energy loss due to exchange of fluids between pores
- Partial saturation increases attenuation due to fluids moving between pores
- In a fully saturated medium there is only extrinsic attenuation due to fracturing
- Saturation increases the density of the material and increases both P- and S-wave velocity
- Shear modulus is independent of fluid saturation
- Dilatency can cause expansion and permeability
- Variation in lithology observed in elastic constants
- Poisson effect—change in shear modulus due to change in fluid properties because of the effect of void

Visualization and Correlation Analysis

We analyzed available, free visualization software that will aid in analysis of results. We identified VisIt (LLNL, 2008) as a useful visualization software. It is a fully interactive three-dimensional visual analysis program that is supported by LLNL. The VisIt development objective was: "to provide a synergy between visual interfaces and databases. Generally, visual interfaces have focused on human capabilities while databases have focused on efficient query processing. Developing a synergy between them will shift us from data workers to data thinkers, people who can use data at the speed-of-thought. VisIt attempts to overcome three problems: (1) ineffective information presentation, (2) poor exploratory capabilities, and (3) difficult user interfaces and database GUIs" (see https://wci.llnl.gov/codes/visit/home.html).

Application of Rock Physics and Effective Medium Theories (EMT) to the Southeast Geysers Geothermal Field

We apply EMT to the southeast Geysers geothermal field, California. This study was unconstrained and did not provide a validation, since actual values are not known, but it demonstrates the applications we are proposing (Berge et al., 2001). Utilizing effective medium theory, we compared three-dimensional V_p and Q_p attenuation parameters for the Geysers Geothermal Field (Zucca et al., 1993) to predicted values from EMT. This led to an "expected" distribution of the velocity with depth in the reservoir. We considered the effects of pressure closing the low-aspect-ratio cracks on V_p exclusively. The mineralogical changes were not dramatic through the reservoir. We then determined the depth where velocity stops increasing and the initial velocity for the "expected" velocity/depth curve from a 1-D inversion of field data. A similar assumption was used for the Q_p vs depth curve. By identifying parts of the reservoir volume that did not match this expected curve, we identified regions that are anomalous either in fracture density and spacing, fluid saturation, or mineralogy.

We chose the following criteria to define "anomalous" areas: V_p differs from the expected value by more than 5% and Q_p differs from the expected value by more than 50%. These criteria were somewhat arbitrary. We did not attempt to determine whether the anomalous values were caused by anomalous fracture density and spacing, saturation differences, or mineralogy differences. Figure 5a shows portions of volume where V_p and Q_p are high, consistent with a reduced fracture density. The anomalies occur at two elevations, about -1000 m, in the melange, and -2000 m, mostly in the felsite. Figure 5b shows portions of volume with high velocity but low Q_p. These occur about -1500 m within the graywacke. This may be a combination of fluid and compositional effects; additional modeling will be required to identify what might cause this type of anomaly. Figure 5c shows areas with low V_p and low Q_p, consistent with a high fracture density. These also occur within the graywacke. No zones were found with low V_p but high Q_p. The high V_p and Q_p anomaly (Figure 5a) is centered on the zone of greatest pressure drop and is mostly within the shallowest part of the felsite and in the malange. The anomalous zones within the graywacke reservoir (Figures 5b and 5c) are on either side of the felsite, in areas of more moderate pressure depletion. Evaluating the relationship of these anomalous zones to structural elements, injection, production, and other factors may show that these factors are diagnostic of important features within the field.

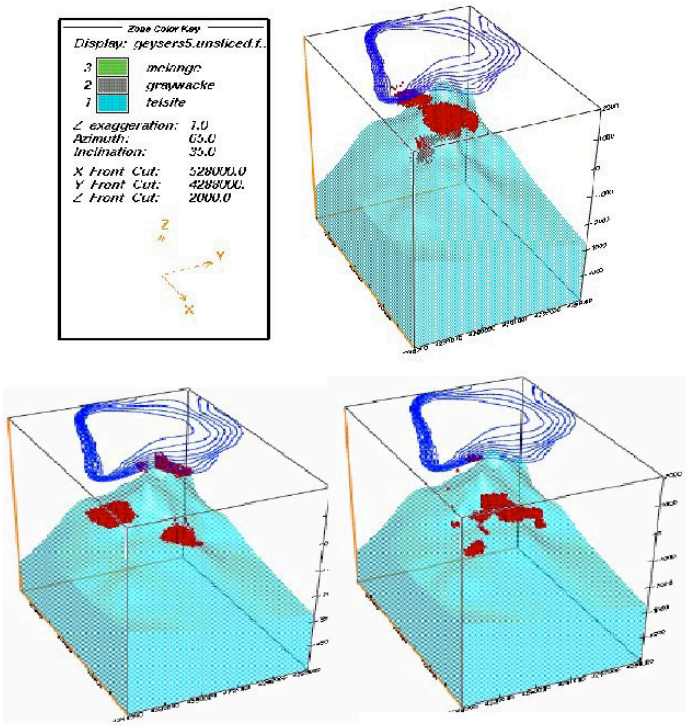

Figure 5. Felsite formation is shown in blue shading and graywacke is above the felsite. Intrusion through greyawacke in red. Pressure contours in blue.

Summary and Conclusions

We have developed a system that rapidly and inexpensively utilizes recordings of micro-earthquakes to provide accurate earthquake locations and image geologic structure; and possibly identify fractures, state of fluids, and permeable zones. Our "Rapid Reservoir Assessment System" (RRAS) is designed to utilize earthquakes within a reservoir environment that occur either naturally or due to fluid injection or production. The system is also ideally suited for monitoring hydro-fracking, since it provides high-resolution earthquake locations.

References

Berryman, J. G. (1995) Mixture theories for rock properties, in Rock Physics & Phase Relations, a handbook of Physical Constants, AGU Reference Shelf 3, Thomas J. Ahrens, Editor, American Geophysical Union, Washington, DC, pp 205-228.

Berryman, James G. (2007) Seismic waves in rocks with fluids and fractures. Geophys. J. Int. 171, 954-974.

Berryman, J.G., P.A. Berge, and B.P. Bonner, 2002. "Estimating Rock Porosity and Fluid Saturation Using Only Seismic Velocities." Geophysics, v. 67, No. 2, p. 391–404.

Berge, Patricia, Lawrence Hutchings, Jeffrey Wagoner, and Paul Kasameyer (2001) Rock Physics Interpretation of P-wave Q and Velocity Structure, Geology, Fluids and Fractures at the Southeast Portion of The Geysers Geothermal Reservoir**.** Geothermal Res. Council, Transactions, 14, 2001 Annual Meeting, San Diego, CA.

Bonner, Brian , Lawrence Hutchings, Pat Berge, and Paul Kasameyer (2011) Rock Physics Interpretations for Reservoir Properties from Microearthquake Recordings. submittal to the Journal of Geophysics.

Bonner, Brian, Lawrence Hutchings, and Paul Kasameyer (2006) A Strategy for Interpretation of Microearthquake Tomography Results in the Salton Sea Geothermal Field Based upon Rock Physics Interpretation of State 2-14 Borehole Logs. Geothermal Res. Council, Transactions, 14, 2007 Annual Meeting, Reno, NV. LLNL, UCRL-PROC-222141.

Daley, T.M., T.V. McEvilly, and E.L. Majer, 1988. "Analysis of P and S Wave Vertical Seismic Profile Data from the Salton Sea Scientific Drilling Project." *J. Geophys. Res.* v. 93, No. B11, p. 13,025–13,036.

Foulger, G.R., Grant, C.C., Ross, A. and Julian, B.R. (1997) Industrially induced changes in Earth structure at The Geysers geothermal area,California. GRL, 24(2): 135-137.

Gassmann, F., 1951. (translated, Berryman, "Origin of Gassmann's Equationis". Geophysics 64. 1627-1629, 1999.

Hutchings, Lawrence (2002) Program NetMoment, a Simultaneous Inversion for Moment, Source Corner Frequency, and Site Specific t*. Lawrence Livermore National Laboratory, UCRL-ID 135693.

Hutchings, Lawrence (2011) Accuracy and Resolution in Earthquake Location and Tomography Studies. Submitted, prodeedings, Geothermal Resources Council Annual Meeting.

Julian, B.R., Ross, A., Foulger, G.R. and Evans, J.R. (1996) Three-dimensional seismic image of a geothermal reservoir: The Geysers,California. GRL, 23(6): 685-688.

Julian, Bruce R., Gillian Foulger, and Keith Richards-Dieger, 1999. The Coso Geothermal Area: A Laboratory for Advanced MEQ Studies for Geothermal Monitoring. Geothermic 42.

Larsen, S., and C. A. Schultz (1995). ELAS3D: 2D/3D elastic finite-difference wave propagation code, *Technical Report No. UCRL-MA-121792*, 19 pp.

Majer, E.L., T.V. McEvilly, F.S. Eastwood, L.R. Myer, 1988. Fracture Detection using P-wave and S-wave Vertical Seismic Profiling at The Geysers. Geophysics 63, 199.

Minson, S. E. and Dreger, D. S. (2008), Stable inversions for complete moment tensors. Geophysical Journal International, 174: 585–592. doi:10.1111/j.1365-246X.2008.03797.x

Thurber, C.H. (1983). Earthquake locations and three-dimensional crustal structure in the Coyote Lake area, central California. J. Geophys. Res., 88, 8226-8236.

Waldhauser, F., & W.L. Ellsworth (2000). A double-difference earthquake location algorithm: Method and applications to the northern Hayward fault. Bull. Seism. Soc. Am., 90, 1353-1368.

Zhang, H. (2003) Double-difference Seismic Tomography Method and its Applications. Ph.D. dissertation, University of Wisconsin-Madison.

Zucca, J.J., L.J. Hutchings, and P.W. Kasameyer, 1994. Seismic Velocity and Attenuation Structure of the Geysers Geothermal Field, California. *Geothermics* 23, 111-126.

Zhang, and C. H. Thurber (2007) Estimating the model resolution matrix for large seismic tomography problems based on Lanczos bidiagonalization with partial reorthogonalization. Geophysical Journal International, pages 337–345, Volume 170, Issue 1.